Interaction of Plasmon and Molecular Resonances for Rhodamine 6G Adsorbed on Silver Nanoparticles

Jing Zhao, Lasse Jensen, Jiha Sung, Shengli Zou,[†] George C. Schatz,* and
Richard P. Van Duyne*

*Contribution from Northwestern University, Department of Chemistry,
Evanston, Illinois 60208-3113*

Received February 5, 2007; E-mail: vanduyne@northwestern.edu; schatz@chem.northwestern.edu

Abstract: Localized surface plasmon resonance (LSPR) is a key optical property of metallic nanoparticles. The peak position of the LSPR for noble-metal nanoparticles is highly dependent upon the refractive index of the surrounding media and has therefore been used for chemical and biological sensing. In this work, we explore the influence of resonant adsorbates on the LSPR of bare Ag nanoparticles ($\lambda_{max,bare}$). Specifically, we study the effect of rhodamine 6G (R6G) adsorption on the nanoparticle plasmon resonance because of its importance in single-molecule surface-enhanced Raman spectroscopy (SMSERS). Understanding the coupling between the R6G molecular resonances and the nanoparticle plasmon resonances will provide further insights into the role of LSPR and molecular resonance in SMSERS. By tuning $\lambda_{max,bare}$ through the visible wavelength region, the wavelength-dependent LSPR response of the Ag nanoparticles to R6G binding was monitored. Furthermore, the electronic transitions of R6G on Ag surface were studied by measuring the surface absorption spectrum of R6G on an Ag film. Surprisingly, three LSPR shift maxima are found, whereas the R6G absorption spectrum shows only two absorption features. Deconvolution of the R6G surface absorption spectra at different R6G concentrations indicates that R6G forms dimers on the metal surface. An electromagnetic model based on quasi-static (Gans) theory reveals that the LSPR shift features are associated with the absorption of R6G monomer and dimers. Electronic structure calculations of R6G under various conditions were performed to study the origin of the LSPR shift features. These calculations support the view that the R6G dimer formation is the most plausible cause for the complicated LSPR response. These findings show the extreme sensitivity of LSPR in elucidating the detailed electronic structure of a resonant adsorbate.

Introduction

The last two decades have witnessed a rapid growth in the development of highly selective and sensitive optical chemical and biological nanosensors.[1,2] Fluorescent and colorimetric dyes are widely used in these applications, where they can be immunoassay labels, tissue stains, and chemical indicators.[3] However, individual dye molecules produce a relatively weak signal (e.g., fluorescein has an absorbance cross section of $3.5 \times 10^{-16} cm^2$),[4] and most fluorescent dyes photobleach, providing only a limited "photon budget."[5] Nanoparticles do not have the same limitations. Noble-metal nanoparticles produce extremely intense scattering and extinction signals (e.g., a single 60-nm silver nanosphere has an extinction cross section of $2.5 \times 10^{-10} cm^2$)[4] and do not photobleach. Adding chemically sensitive dyes to these metal nanostructures produces integrated chemical

sensors with bright, low-bleaching extinction and scattering signals. This paper describes, for the first time, a metal nanoparticle/chromophore coupling with multiple resonant states.

When metal nanoparticles are excited by electromagnetic radiation, they exhibit collective oscillations of their conduction electrons known as localized surface plasmon resonance (LSPR).[6–8] The wavelength (λ_{max}) associated with maximum LSPR extinction of the nanoparticles can be measured with UV–vis spectroscopy. It has been well-established that the LSPR maximum of the nanoparticles strongly depends on the composition, size, shape, and local dielectric environment.[9–11] Therefore, nanoparticles can sense the change in the local refractive index that accompanies molecular binding. Such

[†] Current address: Department of Chemistry, University of Central Florida, Orlando, FL 32816-2366.

(1) Turner, A. P. F. *Science* **2000**, *290*, 1315−1317.
(2) Zhao, J.; Zhang, X.; Yonzon, C. R.; Haes, A. J.; Van Duyne, R. P. *Nanomedicine* **2006**, *1*, 219−228.
(3) Zollinger, H. *Color Chemistry: Syntheses, Properties and Applications of Organic Dyes and Pigments,* 3rd ed.; Wiley-VCH: Weinheim, Germany, 2001.
(4) Yguerabide, J.; Yguerabide, E. E. *Anal. Biochem.* **1998**, *262*, 137−156.
(5) Fraser, S. E. *Nat. Biotechnol.* **2003**, *21*, 1272−1273.

(6) Hutter, E.; Fendler, J. H. *Adv. Mat.* **2004**, *16*, 1685−1706.
(7) Schatz, G. C.; Van Duyne, R. P. Electromagnetic Mechanism of Surface-Enhanced Spectroscopy. In *Handbook of Vibrational Spectroscopy*; Chalmers, J. M., Griffiths, P. R., Eds.; Wiley: New York, 2002; Vol. 1, pp 759−774.
(8) Kreibig, U.; Vollmer, M. *Cluster Materials*; Springer-Verlag: Heidelberg, Germany, 1995; Vol. 25, p 532.
(9) Jensen, T. R.; Duval, M. L.; Kelly, K. L.; Lazarides, A.; Schatz, G. C.; Van Duyne, R. P. *J. Phys. Chem. B* **1999**, *103*, 9846−9853.
(10) Haynes, C. L.; Van Duyne, R. P. *J. Phys. Chem. B* **2001**, *105*, 5599−5611.
(11) Kelly, K. L.; Coronado, E.; Zhao, L.; Schatz, G. C. *J. Phys. Chem. B* **2003**, *107*, 668−677.

nanoparticle-based optical sensing techniques are effective for quantitative detection of chemical and biological targets.[12−19] This is achieved by monitoring the shift in λ_{max} upon binding of the probe analytes onto the nanoparticles.

Most LSPR-sensing experiments have been performed with electronically nonresonant adsorbates, which do not have electronic transitions in the visible wavelength range. However, since many biological targets have visible chromophores, it is worthwhile to broaden the scope of LSPR sensing by exploring electronically resonant adsorbates. Recent progress has revealed the correlation between the molecular resonances and the nanoparticles' surface plasmon resonances for two different resonant adsorbates, [2,3,7,8,12,13,17,18-octakis(propyl)por-phyrazinato]magnesium (II) and iron (II) tris-2,2′-bipyridine.[18] When resonant molecules are adsorbed on the nanoparticles, strong coupling between the molecular resonance and nanoparticle LSPR has been observed experimentally and simulated by electrodynamics theory.[18,20,21] The induced LSPR shift due to this coupling is found to be strongly dependent on the spectral overlap between the molecular resonances and the LSPR. Specifically, a large red-shift occurs when the LSPR is located at a slightly longer wavelength than the molecular resonance, i.e., a factor of 3 greater than when the LSPR is distant from the molecular resonance. On the basis of this amplification mechanism, a nanoparticle-based biosensor has been success-fully developed to detect the binding of a low-molecular weight substrate to cytochrome P450 proteins.[16] By coupling LSPR with the resonant states of these heme-containing proteins, one can monitor the LSPR response to the change in the Soret band of these proteins upon substrate binding.

Rhodamine 6G (R6G) has been chosen in this study because of its active role in surface-enhanced Raman spectroscopy (SERS). It was one of the first molecules used for single-molecule SERS (SMSERS) studies with enhancement as large as 10^{14} to 10^{15} being observed.[22−24] It has been demonstrated that the SERS enhancement factor is closely related to the plasmon resonance of the nanoparticle, laser excitation wave-length, and the molecular resonance.[7,25−29] However, the single-molecule SERS mechanism is not fully understood. Therefore, understanding the coupling of R6G molecular resonances with LSPR is crucial for elucidating the single-molecule SERS mechanism.

In this work, the coupling between the molecular resonances of R6G and the nanoparticles' LSPR is systematically studied by monitoring the change in λ_{max} before and after R6G binding. To explore the wavelength-dependent LSPR shift, nanoparticles with varying λ_{max} through the visible region are fabricated using nanosphere lithography (NSL).[10,30] It is found that the LSPR response is highly wavelength and concentration dependent. In addition, the LSPR response shows extreme sensitivity to all resonant states of the adsorbed species, revealing features difficult to observe using standard absorption methods. By combining theoretical modeling with the experimental observa-tions, a microscopic understanding of the complicated LSPR response is obtained.

Experimental Methods

Materials. Absolute ethanol was obtained from Pharmco (Brookfield, CT). Methanol was purchased from Fisher Scientific (Pittsburgh, PA). Silver wire (99.99%, 0.5 mm diameter) was purchased from D.F. Goldsmith (Evanston, IL). Tungsten vapor deposition boats were acquired from R.D. Mathis (Long Beach, CA). Polystyrene nanospheres with diameters of 280, 390, 450, and 510 nm were received as a suspension in water (Interfacial Dynamics Corporation, Portland, OR or Duke Scientific, Palo Alto, CA) and were used without further treatment. Millipore cartridges (Marlborough, MA) were used to purify water to a resistivity of 18.2 MΩ·cm. Fisherbrand no. 2 glass coverslips with 18-mm diameters were obtained from Fisher Scientific (Pittsburgh, PA). Benzenethiol and rhodamine 6G were obtained from Sigma Aldrich (St. Louis, MO) and used as received.

Substrate Preparation. Glass substrates were cleaned in piranha solution (1:3 30% H_2O_2/H_2SO_4) for 30 min at 80 °C. (**Warning!** Piranha reacts violently with organic compounds and should be handled with caution.) Samples were allowed to cool and were then rinsed profusely with water. Samples were then sonicated in 5:1:1 $H_2O/NH_4OH/30\%$ H_2O_2 and rinsed with water. The samples were stored in ultrapure water prior to use.

Nanoparticle Preparation. NSL was used to create monodispersed, surface-confined Ag nanotriangles.[30−32] Polystyrene nanospheres (~2.2 μL) were drop-coated onto the glass substrates and allowed to dry, forming a monolayer in a close-packed hexagonal formation. This close-packed layer of nanospheres served as a lithographic mask to deposit Ag in the triangular voids between the spheres. The samples were mounted into a Consolidated Vacuum Corporation vapor deposition chamber. A Leybold Inficon XTM/2 quartz crystal microbalance (East Syracuse, NY) was used to measure the thickness of the Ag film deposited over the nanosphere mask. Following metal deposition, the samples were sonicated for 3−5 min in ethanol to remove the polystyrene nanosphere mask. The perpendicular bisector of the nanoparticles was varied by changing the diameter of the nanospheres used. The height of the nanoparticles was varied by depositing varying amounts of Ag onto the sample. These two parameters were varied to alter the LSPR peak position throughout the visible region of the spectrum. In general, an increase in nanosphere diameter and/or a decrease in metal film thickness results in a red-shift in LSPR.

Nanoparticle Solvent Annealing and Functionalization. For each experiment, the sample was stabilized and functionalized in a home-

(12) Haes, A. J.; Chang, L.; Klein, W. L.; Van Duyne, R. P. *J. Am. Chem. Soc.* **2005**, *127*, 2264−2271.
(13) Riboh, J. C.; Haes, A. J.; McFarland, A. D.; Yonzon, C. R.; Van Duyne, R. P. *J. Phys. Chem. B* **2003**, *107*, 1772−1780.
(14) Yonzon, C. R.; Jeoung, E.; Zou, S.; Schatz, G. C.; Mrksich, M.; Van Duyne, R. P. *J. Am. Chem. Soc.* **2004**, *126*, 12669−12676.
(15) Dahlin, A.; Zach, M.; Rindzevicius, T.; Käll, M.; Sutherland, D. S.; Hook, F. *J. Am. Chem. Soc.* **2005**, *127*, 5043−5048.
(16) Zhao, J.; Das, A.; Zhang, X.; Schatz, G. C.; Sligar, S. G.; Van Duyne, R. P. *J. Am. Chem. Soc.* **2006**, *128*, 11004−11005.
(17) McFarland, A. D.; Van Duyne, R. P. *Nano Lett.* **2003**, *3*, 1057−1062.
(18) Haes, A. J.; Zou, S.; Zhao, J.; Schatz, G. C.; Van Duyne, R. P. *J. Am. Chem. Soc.* **2006**, *128*, 10905−10914.
(19) Lin, H. Y.; Chen, C. T.; Chen, Y. C. *Anal. Chem.* **2006**, *78*, 6873−6878.
(20) Ambjornsson, T.; Mukhopadhyay, G.; Apell, S. P.; Käll, M. *Phys. Rev. B* **2006**, *73*, 085421-1-10.
(21) Wiederrecht, G. P.; Wurtz, G. A.; Hranisavljevic, J. *Nano Lett.* **2004**, *4*, 2121−2125.
(22) Nie, S.; Emory, S. R. *Science* **1997**, *275*, 1102−1106.
(23) Futamata, M.; Maruyama, F.; Ishikawa, M. *J. Phys. Chem. B* **2004**, *108*, 13119−13127.
(24) Michaels, A. M.; Nirmal, M.; Brus, L. E. *J. Am. Chem. Soc.* **1999**, *121*, 9932−9939.
(25) Haynes, C. L.; Van Duyne, R. P. *J. Phys. Chem. B* **2003**, *107*, 7426−7433.
(26) McFarland, A. D.; Young, M. A.; Dieringer, J. A.; Van Duyne, R. P. *J. Phys. Chem. B* **2005**, *109*, 11279−11285.
(27) Zhang, X.; Zhao, J.; Whitney, A. V.; Elam, J. W.; Van Duyne, R. P. *J. Am. Chem. Soc.* **2006**, *128*, 10304−10309.
(28) Emory, S. R.; Haskins, W. E.; Nie, S. M. *J. Am. Chem. Soc.* **1998**, *120*, 8009−8010.
(29) Hildebrandt, P.; Stockburger, M. *J. Phys. Chem.* **1984**, *88*, 5935−5944.

(30) Hulteen, J. C.; Van Duyne, R. P. *J. Vac. Sci. Technol., A* **1995**, *13*, 1553−1558.
(31) Haes, A. J.; Zhao, J.; Zou, S.; Own, C. S.; Marks, L. D.; Schatz, G. C.; Van Duyne, R. P. *J. Phys. Chem. B* **2005**, *109*, 11158−11162.
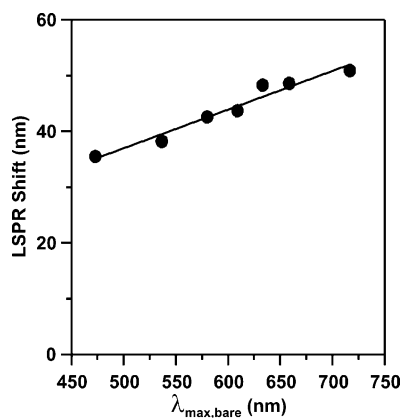(32) Haes, A. J.; Hall, W. P.; Chang, L.; Klein, W. L.; Van Duyne, R. P. *Nano Lett.* **2004**, *4*, 1029−1034.

Figure 1. Wavelength-dependent LSPR shift induced by a monolayer of benzenethiol vs the LSPR wavelength of bare Ag nanoparticles.

built flow cell.[33] Prior to modification, the Ag nanoparticles were solvent annealed[33] with methanol. Dry N_2 gas and solvent were cycled through the flow cell until the λ_{max} of the sample stabilized. Samples were then incubated in R6G ethanolic solutions for 1 h. After incubation, the nanoparticle samples were rinsed with $10-20$ mL of ethanol and dried by flowing N_2 gas through the sample cell.

Ultraviolet−Visible Extinction Spectroscopy. UV−vis extinction spectra were collected using an Ocean Optics (Dunedin, FL) SD2000 or HR2000 fiber-optic coupled spectrometer with a CCD detector. All spectra in this study are macroscopic measurements performed in standard transmission geometry with unpolarized light. The probe spot size was approximately $1-2$ mm in diameter.

Ultraviolet−Visible Surface Absorption Spectroscopy of R6G. UV−vis surface absorption spectra of R6G on thin metal films were collected using an integrating sphere (RSA-HP-84, LabSphere) and fiber-optic coupled spectrometer (USB2000-VIS-NIR, Ocean Optics) with a CCD detector. R6G was adsorbed onto a 200-nm thick Ag film (vapor deposited onto a glass substrate) by immersion in R6G ethanolic solutions at room temperature for 12 h, followed by thorough rinsing in ethanol. Two reflectance spectra were measured. The reference spectrum, reference (λ), was that of an identical 200-nm thick Ag film on glass with no R6G adsorbed. The sample spectrum, sample (λ), was that of R6G on a 200-nm thick Ag film. The surface absorption spectrum was then calculated as $A_{surf}(\lambda) = -\log_{10}$ (sample(λ)/reference (λ)). All the measurements were conducted in air at room temperature.

Results and Discussion

Wavelength Dependence of Benzenethiol-Induced LSPR Shift. To explore the wavelength dependence of the adsorbate-induced LSPR shift, a nonresonant adsorbate, benzenethiol, was investigated. Nanoparticles with various heights and widths were fabricated by NSL.[34] The extinction spectra of the nanoparticles before and after exposure to benzenethiol were collected in a N_2 environment. As the aspect ratio (in-plane width/out-of-plane height) of the nanoparticles increases from 1.3 to 2.9, the LSPR of bare nanoparticles varies from ~460 nm to ~730 nm. The effect of a monolayer of benzenethiol on the LSPR ($\Delta\lambda_{max}$) versus the LSPR wavelength of bare nanoparticles ($\lambda_{max,bare}$) was monitored and plotted in Figure 1. From Figure 1, the LSPR shift increases monotonically from 35 to 55 nm with increasing $\lambda_{max,bare}$. This agrees with previous observations, showing that with increasing aspect ratio of the nanoparticle, the LSPR shift increases.[14]

Wavelength Dependence of the R6G-Induced LSPR Shift. Parts A and B of Figure 2 show the structure of R6G and its solution absorption spectrum, respectively. In ethanol solution (solid green line in Figure 3A), R6G exhibits a peak at 530 nm from the S_0-S_1 electronic transition (extinction coefficient ϵ_{max} = 105 $mM^{-1}\cdot cm^{-1}$, fwhm = 31.85 nm, 1145 cm^{-1}) and a shoulder at 495 nm from vibronic S_0-S_1 transition.[29,35]

The LSRP shift induced by resonant adsorbates is known to be highly wavelength dependent. Figure 3A reveals the influence of a monolayer of R6G on the LSPR wavelength of Ag nanoparticles. The electronic absorption spectrum of R6G has been included for direct comparison with the experimental data points. The LSPR shift displays interesting behavior when scanning $\lambda_{max,bare}$ from 450 to 750 nm. When $\lambda_{max,bare}$ is much bluer (i.e., $450-470$ nm) than the molecular resonance, a small LSPR shift (less than 5 nm) is observed. As $\lambda_{max,bare}$ is gradually tuned to the red, an increase in the induced shift is found. A local LSPR shift maximum of 20 nm occurs at $\lambda_{max,bare} \approx 500$ nm. When $\lambda_{max,bare}$ approaches the molecular resonance at 530 nm, the induced LSPR shift gradually decreases in the range of $500-530$ nm. When $\lambda_{max,bare}$ is very close to the molecular resonance, the LSPR shift drops, and a slight blue shift (~5 nm) is observed (Figure 3B). Although minima in wavelength-shift plots similar to what we find in the $520-530$-nm range were seen in an earlier study of resonant chromophores on metal particles,[18] this is the first time that a blue-shift has been observed. In the past work it was noted that minima are found on the blue side of the molecular resonance, as this is where the molecular polarizability is negative, leading to an induced polarization that destructively interferes with the oscillating polarization associated with plasmon resonance excitation. Whether this leads to a blue shift is likely determined by the size of the adsorbate polarizability and whether this dominates over other contributions to the adlayer polarizability (from molecules that are not in resonance) which would typically be positive.

When $\lambda_{max,bare}$ is shifted red from the molecular resonance at 530 nm, the LSPR shift gradually recovers from $530-575$ nm and reaches a maximum value of 55 nm at $\lambda_{max,bare} \approx 575$ nm. This maximum response is amplified by ~300% over the average LSPR shift (~20 nm) (Figure 3C). Maxima similar to this were seen previously for other molecules,[16,18] and their occurrence was explained based on the fact that both the molecular and metal polarizability is positive on the red side of the molecular resonance.

As $\lambda_{max,bare}$ is further red-shifted from 575 to 590 nm, the LSPR shift sharply drops to a less than 10-nm shift followed by another LSPR shift maximum (~50 nm) at $\lambda_{max,bare} \approx 595$ nm (Figure 3D). Finally, when $\lambda_{max,bare}$ is red-shifted past 595 nm, the LSPR shift slowly decreases to less than 10 nm at $\lambda_{max,bare}$ close to 700 nm (Figure 3E). Notice that the LSPR shifts induced by R6G at off-resonance wavelengths (<470 nm and >650 nm) are small compared to the shifts induced by benzenethiol. This simply reflects the lower packing density of R6G compared to that of benzenethiol due to its larger size. Furthermore, unlike in the previously reported studies,[18] the LSPR peak intensity and width do not change significantly over the scanned wavelength region.

(33) Malinsky, M. D.; Kelly, K. L.; Schatz, G. C.; Van Duyne, R. P. *J. Am. Chem. Soc.* **2001**, *123*, 1471−1482.
(34) Jensen, T. R.; Malinsky, M. D.; Haynes, C. L.; Van Duyne, R. P. *J. Phys. Chem. B* **2000**, *104*, 10549−10556.

(35) Soper, S. A.; Nutter, H. L.; Keller, R. A.; Davis, L. M.; Shera, E. B. *Photochem. Photobiol.* **1993**, *57*, 972−977.
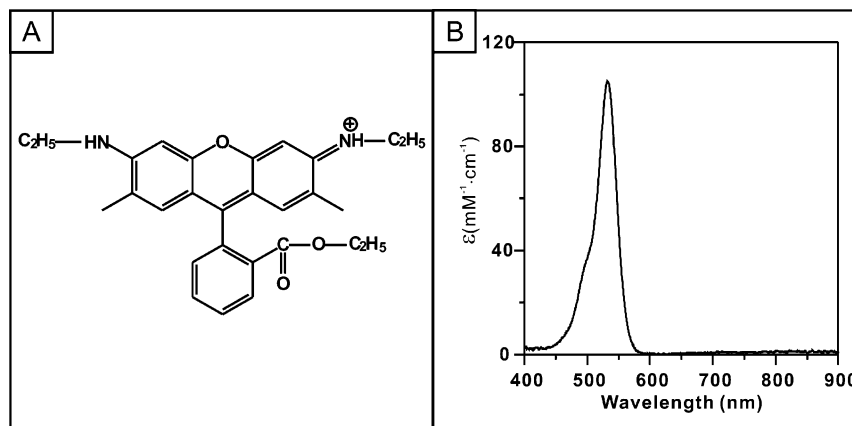
Figure 2. (A) Molecular structure of R6G. (B) Absorption spectrum of R6G in ethanol solution.
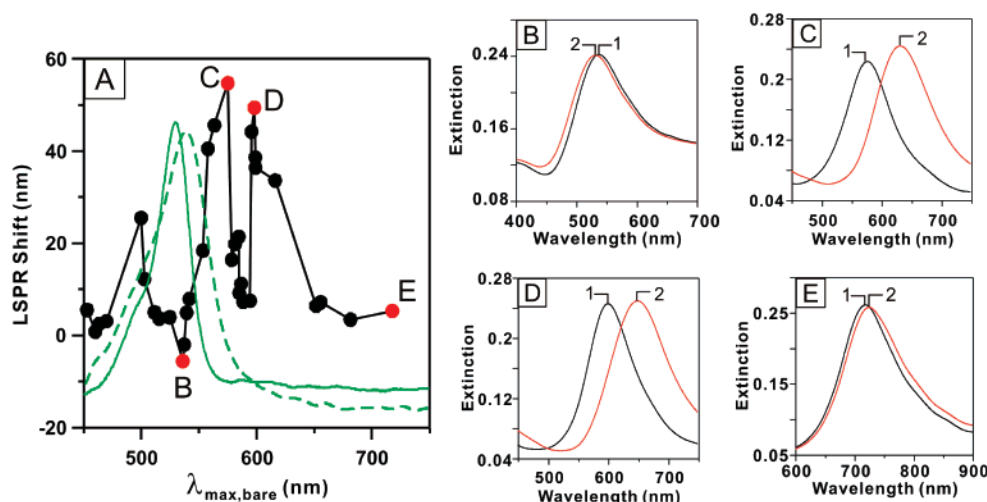

Figure 3. Influence of R6G on the LSPR shift of Ag nanoparticles and representative LSPR spectra. (A) Wavelength-dependent LSPR shift induced by a monolayer of R6G vs the LSPR wavelength of bare Ag nanoparticles. Solid black line with filled dots is a plot of the LSPR shift (nm) vs LSPR position of Ag nanoparticles. Solid green line is the absorption spectrum of the R6G in ethanol solution (arbitrary scaling). Green dashed line is the absorption spectrum of the R6G on a 200 nm Ag film (arbitrary scaling). (B) LSPR spectra of Ag nanoparticles (associated with point C in Figure A) before chemical modification (black line), $\lambda_{max} = 535.9$ nm, and after modification with R6G (red line), $\lambda_{max} = 530.3$ nm. The LSPR shift $= -5.6$ nm, % fwhm $= 1.1$%, and % $I = -5.9$%. (C) LSPR spectra of Ag nanoparticles (associated with point B) in Figure A before chemical modification (1) $\lambda_{max} = 575.0$ nm, and after modification with R6G (2) $\lambda_{max} = 629.7$ nm. The LSPR shift $= 54.7$ nm, % fwhm $= 3.4$%, and % $I = +11.9$%. (D) LSPR spectra of Ag nanoparticles (associated with point D in Figure A) before chemical modification (1) $\lambda_{max} = 598.0$ nm, and after modification with R6G (2) $\lambda_{max} = 647.4$ nm. The LSPR shift $= 49.4$ nm, % fwhm $= 8.9$%, and % $I = +1.5$%. (E) LSPR spectra of Ag nanoparticles (associated with point E in Figure A) before chemical modification (black line) $\lambda_{max} = 717.8$ nm, and after modification with R6G (red line) $\lambda_{max} = 723.1$ nm. The LSPR shift $= 5.3$ nm, % fwhm $= 8.6$%, and % $I = -1.8$%.

It is especially noteworthy that three LSPR shift maxima have been observed, whereas there are only two absorption features in the molecular electronic transitions. This phenomenon is different from what was observed in previous wavelength-shift spectroscopy studies near molecular resonances, where only one LSPR shift maximum was observed.[18]

Empirical Model of the Wavelength Shift. The LSPR shift is dependent on the refractive index of the surrounding medium of the nanoparticle. For nonresonant adsorbates, the LSPR wavelength shift ($\Delta\lambda_{max}$) can be estimated from the following empirical equation:[13,16,18]

$$\Delta\lambda_{max} = m(n_{ads} - n_{N_2})(1 - e^{-2d/l_d}) \qquad (1)$$

where m is the refractive index sensitivity of the nanoparticles ($\sim$200 nm/RIU),[18,33] n_{ads} is the real part of the refractive index

of the adsorbate, n_{N2} is the refractive index of the N$_2$ surroundings (1.0), d is the molecular thickness (experimentally determined to be 1.0 nm by measuring the particle height before and after R6G adsorption using atomic force microscopy, data not shown), and l_d is the characteristic electromagnetic field decay length of the nanoparticles (approximately 6 nm).[13] For resonant adsorbates, it has been demonstrated that $\Delta\lambda_{max}$ near molecular resonance can be estimated from the real part of the refractive index using a Kramers−Kronig transformation[37] and eq 1. Using the same treatment as in the previous studies, n_{ads} is expressed as the sum of the nonresonant part of the refractive index ($n_{non,ads}$) and the resonant contribution ($\Delta n_{res,ads}$). From eq 1, the refractive index of the adsorbate layer can be estimated. Since the average $\Delta\lambda_{max}$ at off-molecular resonance wavelengths is 10 nm, the $n_{non,ads}$ of the R6G monolayer is calculated to be $\sim$1.35.

(36) Jung, L. S.; Campbell, C. T.; Chinowsky, T. M.; Mar, M. N.; Yee, S. S. *Langmuir* **1998**, *14*, 5636−5648.

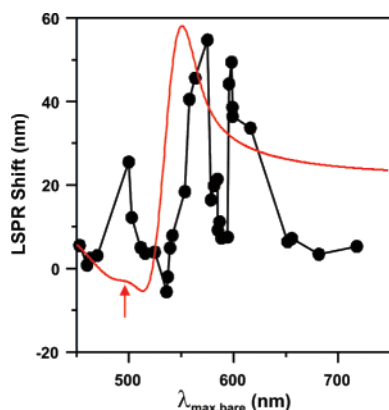(37) Kronig, R. De L.; Kramers, H. A. *Z. Phys.* **1928**, *48*, 174−179.

Figure 4. Predicted LSPR shift (using eq 1) with a scaled refractive index from Kramers−Kronig analysis. The solid black line with filled dots is a plot of the experimental LSPR shift (nm) vs spectral position of the bare Ag nanoparticles.

Using a Kramers−Kronig transformation, $\Delta n_{res,ads}$ of R6G was transformed from its solution absorption spectrum (Figure 2B) using the following equation:[37,38]

$$\Delta n_{res,ads}(\omega) = \frac{c}{\pi} \int_0^\infty \frac{\Delta\alpha(\omega')}{(\omega')^2 - \omega^2} d\omega' \qquad (2)$$

where $\Delta\alpha$ is the change in the absorption coefficient (2.303· $A(\lambda)/T$ in which $A(\lambda)$ is the molecular absorbance at a given wavelength and T is the effective molecular thickness), c is the speed of light, λ is the wavelength of light, and ω is the angular frequency ($2\pi c/\lambda$). The Kramers−Kronig transformation expresses the real part of the refractive indices as an integral of the absorption coefficients. Notice that the integral in this formula has a singularity, which was treated numerically by excluding the singular point in the integral. This treatment will lead to some uncertainty in the absolute value of the refractive indices; however, it will simply result in a different scaling factor than what is used in the following sections to predict the LSPR shift. Therefore, the overall line shape of the predicted LSPR shift will not be affected.

Figure 4 shows the LSPR shift predicted using eq 1. The predicted LSPR shift has a maximum at 550 nm and a minimum at 520 nm associated with the S_0-S_1 transition, and the very small peak at 500 nm (indicated by the arrow in Figure 4) is associated with the vibronic band. This model fails to predict the complicated LSPR shift features. Although it captures two of the experimental LSPR shift features to some extent, the position and magnitude of the two features do not agree with the experiments. The additional LSPR shift maximum at ∼595 nm is not predicted using this empirical model. According to the empirical analysis, another absorption feature at ∼570 nm is necessary to generate such LSPR shift results.

Concentration Dependence of the R6G Absorbance on Ag Film and Analysis. As discussed, R6G has two absorption features in ethanol solution: an S_0-S_1 electronic transition and a vibronic shoulder. Figure 5A shows the deconvolution of the R6G solution-phase absorption spectrum with two Gaussian curves at 532 and 504 nm. Since all the R6G-induced LSPR shift measurements were conducted on an Ag surface with nanoscale patterns, it is important to examine the absorption
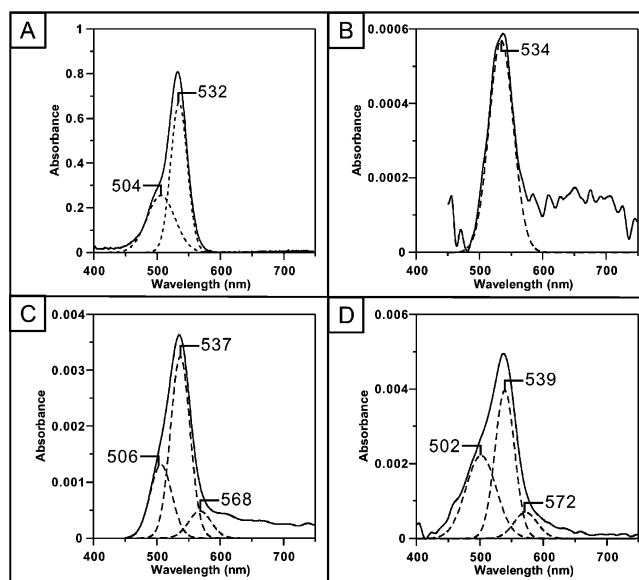
(38) Bohren, C. F.; Huffman, D. R. *Absorption and Scattering of Light by Small Particles*; Wiley-Interscience: New York, 1983.

Figure 5. Absorption spectra of R6G in ethanol solution and different concentrations of R6G on a Ag surface. Dashed lines represent deconvolution of the spectra into Gaussian bands. (A) R6G in ethanol, (B) 0.6 μM R6G on Ag surface, (C) 6 μM R6G on Ag surface, (D) 0.1 mM R6G on Ag surface.

behavior of R6G on an Ag surface. Ideally, one should study the R6G absorbance on Ag nanoparticles. However, the LSPR extinction always would interfere with the measurements. Instead, an alternative approach is to conduct the optical absorbance measurement of R6G on a continuous Ag film.

Parts B−D of Figure 5 show the absorbances of different dosing concentrations of R6G (0.6 μM, 6 μM and 0.1 mM, respectively) on an Ag surface. R6G is known to form dimers in solution at high concentrations and when intercalated in heterogeneous materials such as clays, silica, and colloidal gold nanoparticles.[39−44] R6G can form both J-type (head-to-tail dipole moments) and H-type dimers (parallel dipole moments). The latter conformer is expected to be more likely on a surface due to the adsorption of R6G through one of its N atoms. The formation of dimers will affect the absorption characteristics of R6G by inducing spectral shifts and band splitting. These changes can be qualitatively explained by exciton theory[45,46] based on interactions between the dipole moments of the monomeric units. The dipole−dipole interactions result in a splitting of the monomer excitation which depends on the geometry of the aggregates. The geometry with the head-to-tail transition dipoles leads to a decrease in energy, and the geometry with the parallel transition dipoles leads to an increase in energy (see the exciton energy diagram in Figure 6). Therefore, the absorption of H-type dimers is predicted to blue-

(39) Martínez, A. M.; Arbeloa, F. L.; Prieto, J. B.; Arbeloa, I. L. *J. Phys. Chem. B* **2005**, *109*, 7443−7450.
(40) Martínez, A. M.; Arbeloa, F. L.; Prieto, J. B.; López, T. A.; Arbeloa, I. L. *J. Phys. Chem. B* **2004**, *108*, 20030−20037.
(41) Martínez, A. M.; Arbeloa, F. L.; Prieto, J. B.; López, T. A.; Arbeloa, I. L. *Langmuir* **2004**, *20*, 5709−5717.
(42) Noginov, M. A.; Vondrova, M.; Williams, S. M.; Bahoura, M.; Gavrilenko, V. I.; Black, S. M.; Drachev, V. P.; Shalaev, V. M.; Sykes, A. *J. Opt. A: Pure Appl. Opt.* **2005**, *7*, S219−S229.
(43) Dare-Doyen, S.; Doizi, D.; Guilbaud, P.; Djedaini-Pilard, F.; Perly, B.; Millie, P. *J. Phys. Chem. B* **2003**, *107*, 13803−13812.
(44) Reisfeld, R.; Zusman, R.; Cohen, Y.; Eyal, M. *Chem. Phys. Lett.* **1988**, *147*, 142−147.
(45) Kasha, M. *Radiat. Res.* **1963**, *20*, 55−70.
(46) Kasha, M.; Rawls, H. R.; El-Bayoumi, M. A. *Pure Appl. Chem.* **1965**, *11*, 371−92.
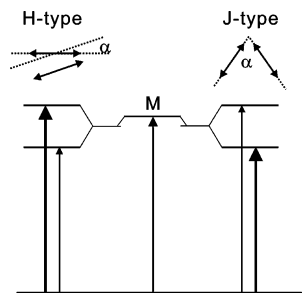
Figure 6. Exciton splitting diagram of the electronic states for R6G monomer and two types (H or J) of dimers, according to the arrangement of the dipole moments. M represents the R6G monomer excitation. H-type and J-type splitting results in an increase or decrease in the excitation energy. The thickest arrow represents the strongest transition.

shift the R6G absorption, and the absorption of J-dimers is predicted to red-shift. To examine whether there is R6G dimer formation on the Ag surface, each absorption spectrum is deconvoluted by different numbers of Gaussian curves with correlation coefficients greater than 0.99. As shown in Figure 5B, when the R6G dosing concentration is as low as 0.6 μM, a weak absorption spectrum is collected and the major absorption band can be fitted with one Gaussian curve at 534 nm. Although there are a few longer wavelength features, the signal-to-noise ratio is not high enough to resolve those peaks. Compared to the R6G solution absorption in Figure 5A, the major absorption band is slightly red-shifted and broadened. Notice that the S_0-S_1 vibronic shoulder observed in solution cannot be resolved when R6G adsorbs on the surface at this dosing concentration. When the R6G dosing concentration is 6 μM, the absorbance of R6G is stronger and broadened compared to absorbance at lower dosing concentration, indicating that the R6G coverage on Ag surface is higher. For the higher R6G dosing concentrations (Figure 5C,D), three Gaussian curves are necessary to generate a good deconvolution of the absorption spectra. Figure 5C shows the deconvolution of this absorption spectrum using three Gaussian curves at 506, 537, and 568 nm. The curve at 537 nm has the highest intensity, followed by the curve at 506 nm, and the lowest intensity at 568 nm. Notice that the major absorption is red-shifted from the R6G solution absorption. The ratio of the 506- to 537-nm bands is 0.41, higher than that of the 504- and 532-nm bands for the solution case (0.38). When the R6G dosing concentration is 0.1 mM, the absorption of R6G increases and broadens further compared to those at the lower concentrations. Figure 5D shows the deconvolution of the absorption spectrum using three Gaussian curves at 502, 539, and 572 nm. The peak at 539 nm has the highest intensity, followed by the curve at 502 nm, and the lowest intensity at 572 nm. Notice that the major absorption is shifted further to the red from the R6G solution absorption. The ratio of the 502- to 539-nm bands further increases to 0.56. Since the spectral positions of the dimer band and the vibronic shoulder of the monomer overlap, it is not possible to distinguish them. However, it is known from the solution and intercalation experiments that an increase in the ratio of the band at ∼500 nm and the band at ∼540 nm and a shifting in the position of these bands are evidence for dimer formation.[39−44] The increase in the ratio of these two bands with increasing concentration observed here, therefore, suggests that R6G dimer formation on the Ag surface is evident. Note that different concentrations of R6G were used to dose the surface due to the morphology

difference of the Ag nanoparticles and films. The NSL-fabricated nanoparticles are more likely to encourage the R6G dimer formation at a lower concentration. Higher concentration of R6G dosing solution could be used, but past studies show that R6G tends to form dimers in ethanol solution when its concentration is higher than 0.1 mM, thus introducing interference from R6G dimers already formed in the solution.[47]

Concentration Dependence of the R6G-Induced LSPR Shift. From the above discussion, it is clear that the absorbance of R6G on an Ag surface is concentration dependent. It is therefore worthwhile to quantitatively study the effect of a submonolayer coverage of R6G on the LSPR shift. As described in the Experimental Methods, 0.6 μM R6G is used to ensure monolayer coverage with 1 h incubation time. By keeping the same incubation time, the effect of a submonolayer of R6G on the LSPR of the Ag nanoparticles is studied by varying the R6G concentration. Since the LSPR shift is highly wavelength dependent, two representative plasmon wavelengths of the bare nanoparticles are chosen: one at ∼540 nm, which is slightly red of the molecular resonance, and the other at ∼560 nm, which is close to the wavelength of the maximum LSPR shift observed in Figure 3A.

The LSPR shift versus the concentration of R6G is plotted in Figure 7. The data shown in Figure 7A represent the LSPR shift when $\lambda_{max,bare}$ is at 540 nm and those in Figure 7B represent the LSPR shift when $\lambda_{max,bare}$ is at 560 nm. From Figure 7A, when the concentration of R6G is as low as 0.006 μM, no shift is observed. As the concentration is gradually increased, the induced LSPR shift increases. When the R6G concentration is 0.3 μM, a maximum LSPR shift of 55 nm is observed. Interestingly, as the concentration further increases, the LSPR shift gradually decreases to less than 10 nm at a concentration of 0.6 μM. Further increase in concentration gives the same LSPR shift which confirms that the nanoparticle surface is saturated with a R6G monolayer. By contrast, the LSPR shifts plotted in Figure 7B do not exhibit such behavior. As the concentration increases, the LSPR shift gradually increases and saturates at 0.6 μM. An explanation for the concentration dependence of LSPR shifts will be presented in the following section.

Electrodynamics Model of the Wavelength Shift. Three R6G absorption bands are observed on the Ag surface, which are probably associated with different R6G monomer and dimers. We calculated refractive indices of the R6G monomer and dimers from the Kramers−Kronig analysis using the deconvoluted curves in Figure 5D. This set of refractive indices is chosen to match these experimental results because they best represent the saturated R6G surface absorption response. Two types of R6G dimers, the H-dimer and J-dimer, are assumed to form on the surface, and these lead to a blue- and red-shift of the absorption peak, respectively, relative to the monomer wavelength. We assign the blue-shifted peak of the deconvoluted curves in Figure 5D as an H-dimer absorption and the red-shifted peak as a J-dimer absorption. Figure 8 shows the predicted LSPR wavelength shift ($\Delta\lambda_{max}$) from eq 1 using the real parts of the refractive indices of the R6G monomer and two dimers. (The refractive indices of R6G monomer and two dimers are available in the Supporting Information.) The three curves in Figure 8

(47) Ojeda, P. R.; Amashta, I. A. K.; Ochoa, J. R.; Arbeloa, I. L. *J. Chem. Soc., Faraday Trans. 2* **1988**, *84*, 1−8.
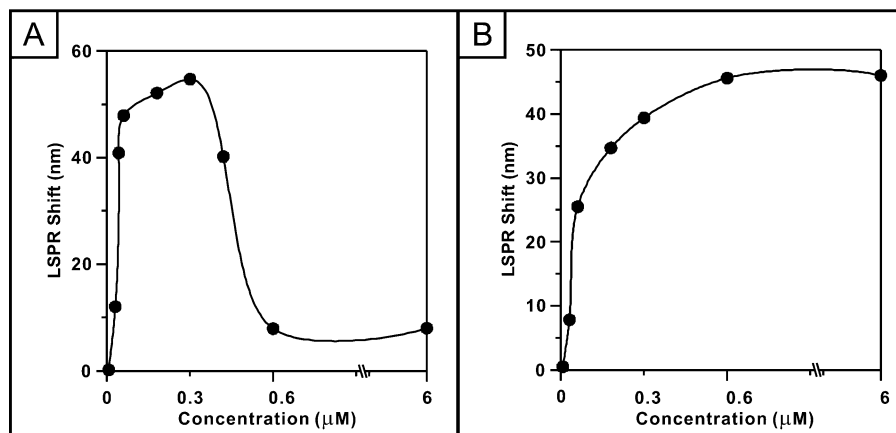
Figure 7. LSPR shift vs concentrations of R6G dosing solutions at constant LSPR of the bare Ag nanoparticles. (A) The LSPR of the bare Ag nanoparticles is ~540 nm. (B) The LSPR of the bare Ag nanoparticles is ~560 nm.
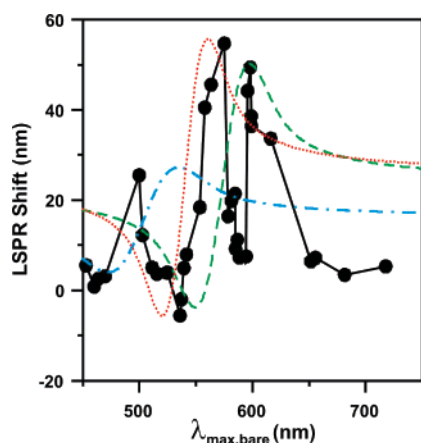

Figure 8. Predicted LSPR shift (using eq 1) with arbitrarily scaled refractive indices from Kramers−Kronig analysis. The solid black line with filled dots is a plot of the experimental LSPR shift (nm) vs spectral position of the Ag nanoparticles. The blue dashed−dotted line, red dotted line, and green dashed line represent the predicted LSPR shift using the refractive indices of the R6G H-dimer, monomer, and J-dimer, respectively.

are arbitrarily scaled (with a scaling factor of 2, 2, and 10 for monomer, H-dimer, and J-dimer, respectively) due to the uncertainty of the coverage of R6G monomer and dimers on the surface. From Figure 8, it is clear that the curves associated with the R6G monomer and dimers correspond to the three experimental LSPR shift features. Nevertheless, the line shape and peak position of the predicted LSPR shift curves do not track the details of the experimental results.

The above empirical model only considered the contribution from the real part of the refractive indices of the R6G monomer and dimers. An advanced electromagnetic method, such as the discrete dipole approximation method,[48,49] including both the real and imaginary parts of the adsorbates' dielectric constants, is needed to reveal the overall effect of the adsorbates. However, such calculations are very computation intensive and time-consuming. As an alternative, we use quasi-static (Gans) theory as a simplified model wherein the particle shape is assumed to be an oblate spheroid.[50] This approach leads to the following expression for the

extinction cross section C_{ext} of a metallic particle in a homogeneous medium:[38,50]

$$C_{ext} \propto Im\left\{\frac{\epsilon_{Ag} - \epsilon_m}{\epsilon_{Ag} + \chi\epsilon_m}\right\} \qquad (3)$$

where ϵ_{Ag} is the dielectric constant of Ag, ϵ_m is the dielectric constant of the surrounding medium, and χ is a shape factor for the particle that has the value 2 for a sphere, and increases with increasing aspect ratio. In the present application, we use χ as a parameter to tune the plasmon resonance wavelength, so the quantitative connection between χ and the structure of the particle is not needed.

For the bare Ag particle, ϵ_m is set to be 1 for N_2. When χ varies from 2.0 to 24.0, the extinction maximum wavelength of the bare Ag particle ($\lambda_{max,bare}$) varies from 400 to 750 nm. It is hypothesized that one of the three R6G structures, i.e., the monomer or one of the two dimers, dominates the LSPR shift at each wavelength; therefore, ϵ_m for the adsorbates ($\epsilon_{m,ads}$) is expressed using the following function:

$$\epsilon_{m,ads} = \begin{cases} \epsilon_H & 400 < \lambda_{max,bare} < 530 \\ \epsilon_{mon} & 530 < \lambda_{max,bare} < 570 \\ \epsilon_J & 570 < \lambda_{max,bare} < 750 \end{cases} \qquad (4)$$

where ϵ_H, ϵ_{mon}, and ϵ_J are the dielectric constants of the R6G H-dimer, monomer and J-dimer, respectively. Values for these dielectric constants were obtained by Kramers−Kronig transformation as noted above. Furthermore, eq 3 applies when the particle is in a homogeneous environment; however, in the experiments, the particles are coated with a very thin layer of R6G, and the rest of the medium is N_2. This inhomogeneous medium is treated using effective medium theory[8,51] ($\epsilon_{m,effective} = \epsilon_m \cdot x + (1 - x) \cdot \epsilon_{N_2}$, where $0 < x < 1$, and x is chosen differently for ϵ_H, ϵ_{mon}, and ϵ_J to match the experiments. x is chosen as for 0.3, 0.05, and 0.9 for ϵ_H, ϵ_{mon}, and ϵ_J to match the experimental LSPR shifts line shape). Plugging $\epsilon_{m,effective}$ into eq 3, the extinction maximum of the Ag particle embedded in R6G ($\lambda_{max,R6G}$) for each χ value is obtained. The LSPR shift is then calculated from the difference between $\lambda_{max,bare}$ and $\lambda_{max,R6G}$ and then is scaled up to match the magnitude of the experimental LSPR shifts by factors of 6, 1, and 2 for R6G

(48) Draine, B. T.; Flatau, P. J. *J. Opt. Soc. Am. A* **1994**, *11*, 1491−1499.
(49) Jensen, T.; Kelly, L.; Lazarides, A.; Schatz, G. C. *J. Cluster Sci.* **1999**, *10*, 295−317.
(50) Mie, G. *Ann. Phys. (Weinheim)* **1908**, *25*, 377−445.

(51) Malinsky, M. D.; Kelly, K. L.; Schatz, G. C.; Van Duyne, R. P. *J. Phys. Chem. B* **2001**, *105*, 2343−2350.
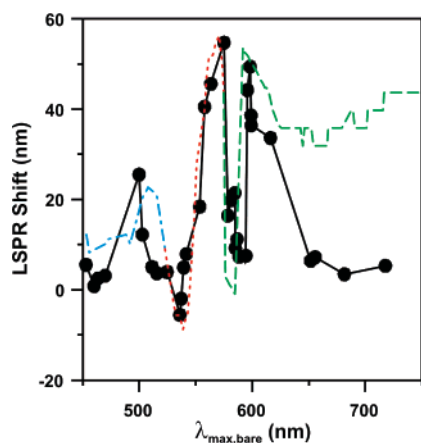
Figure 9. Predicted LSPR shift using eq 3. The solid black line with filled dots is a plot of the experimental LSPR shift (nm) vs spectral position of the Ag nanoparticles. The blue dashed−dotted line, red dotted line, and green dashed line represent the predicted LSPR shift using the dielectric constants of the R6G H-dimer, monomer, and J-dimer, respectively.

monomer, H-dimer, and J-dimer, respectively. This scaling corrects for deficiencies of the Gans model which typically will underestimate dielectric shifts since there are no sharp features on the spheroidal particles.

Figure 9 shows the resulting LSPR shift versus $\lambda_{max,bare}$. The blue dashed−dotted line, red dotted line, and green dashed line represent the predicted LSPR shift using the dielectric constants of the R6G H-dimer, monomer, and J-dimer, respectively. From Figure 9, the predicted LSPR shift agrees well with the experimental data. This illustrates that the three LSPR shift features are associated with R6G in the three different forms. This can be understood if we assume that each particle is primarily coated with one of the three forms of R6G, and then there is a random mixture of the three different kinds of particles. We also considered an effective medium model in which each particle is assumed to be coated with a random mixture of the three R6Gs, so that the adsorbate dielectric constant is a weighted average of the three values; however, this did not match the measurements.

The quasi-static model can also be applied to simulate the concentration-dependent LSPR shifts in Figure 7 by fixing χ for two different initial LSPR wavelengths and varying x in the effective medium treatment. When this is applied at 560 nm, where the R6G monomer absorption dominates, we find that the LSPR shift increases with increasing concentration much the same as shown in Figure 7B, as increasing concentration produces a higher effective dielectric constant in the surrounding medium. On the other hand, the complicated concentration dependence at 540 nm (Figure 7A) can only be understood if we assume that there is a switch in the dominant adsorbed species as concentration is increased. Thus, the portion of the curve in Figure 7A below 0.4 μM would correspond to one species (such as the H-dimer), and then there is a switch to another species (such as the monomer) at higher concentration.

Quantum Chemical Modeling of the Absorption Spectra of Rhodamine 6G. Although the empirical modeling qualitatively reproduces the LSPR shift, it is worthwhile to study the microscopic origin of the R6G absorption features using electronic structure theory. The electronic states of R6G were calculated within time-dependent density functional theory (TD-DFT) using the Amsterdam Density Functional (ADF) program package.[52,53] The Becke−Perdew (BP86) XC-potential,[54,55] and a triple-ζ polarized Slater type (TZP) basis set from the ADF basis set library have been used. The following possible origins of the LSPR shift maximum at ∼595 nm have been examined: (1) formation of R6G dimers, (2) metal−molecule charge-transfer transitions, (3) the change of the angle between the xanthene plane and the phenyl substituent of R6G.

The optimized R6G structure (shown in Figure 10A) was taken from previous work,[56] where the simulated Raman spectrum is in good agreement with the experimental spectrum. The S_0-S_1 transition of R6G corresponds to an excitation from the highest occupied molecular orbital (HOMO) to the lowest unoccupied molecular orbital (LUMO), where both orbitals are localized in the xanthene chromophore and the nitrogen of the ethylamino side groups. The transition is therefore expected to be sensitive to any perturbation on the xanthene ring. The S_0-S_1 transition is calculated to be at 474 nm in vacuum, and a weaker S_0-S_2 transition is at 416 nm. Notice that the calculated S_0-S_1 transition is ∼60 nm blue-shifted from the experimental measurement in solution at 530 nm. Only small changes in the simulated absorption spectrum were found by using larger basis sets and different functionals. Previously, we found that the agreement with experiments was significantly improved by considering solvent effects directly in the calculations.[56] For simplicity, the solvent effects in this work are accounted for by applying a constant red-shift of 56 nm to the calculated values (simulated spectrum shown in Figure 10B). This value is added to all the calculated spectra discussed below.

To examine the exciton splitting in R6G, we calculated the absorption spectra of an antiparallel H-dimer separated by 3.5 Å and a J-dimer with a center-to-center separation of 13.5 Å (structures and spectra shown in Figure 11). For the H-dimer a slight blue-shift (less than 10 nm) of the main transition is observed, which agrees with the shift direction observed experimentally but underestimates the shift magnitude. In addition, a small band at 565 nm is found in the simulated dimer absorption spectrum; however, it has very small oscillator strength. In the case of the J-dimer an 8-nm red-shift of the main transition is found with a weaker transition around 500 nm. In addition, the main J-dimer transition is stronger than the corresponding H-dimer transition. These results are in very good agreement with the expectation from simple exciton theory. For both dimers, the calculated exciton splitting is smaller than that from experimental observation.[39−44] However, the structures for the dimers adopted in the calculation are highly idealized, and it is quite likely one would obtain a better agreement with the experiments by optimizing the dimer structures. The calculations support the findings in the concentration-dependent absorption study of R6G adsorbed on an Ag film. Therefore, the formation of dimers provides a very plausible explanation for the LSPR-shift experiments, especially considering that R6G tends to form dimers in constrained systems.

As a second explanation of the results in Figure 3, we consider the possibility that new transitions, metal−molecule charge-

(52) ADF: Density Functional Theory (DFT) Software for Chemists. http://www.scm.com (accessed 2006).
(53) Velde, G. T.; Bickelhaupt, F. M.; Baerends, E. J.; Guerra, C. F.; Van Gisbergen, S. J. A.; Snijders, J. G.; Ziegler, T. *J. Comput. Chem.* **2001**, *22*, 931−967.
(54) Becke, A. D. *Phys. Rev. A* **1988**, *38*, 3098−3100.
(55) Perdew, J. P. *Phys. Rev. B* **1986**, *33*, 8822−8824.
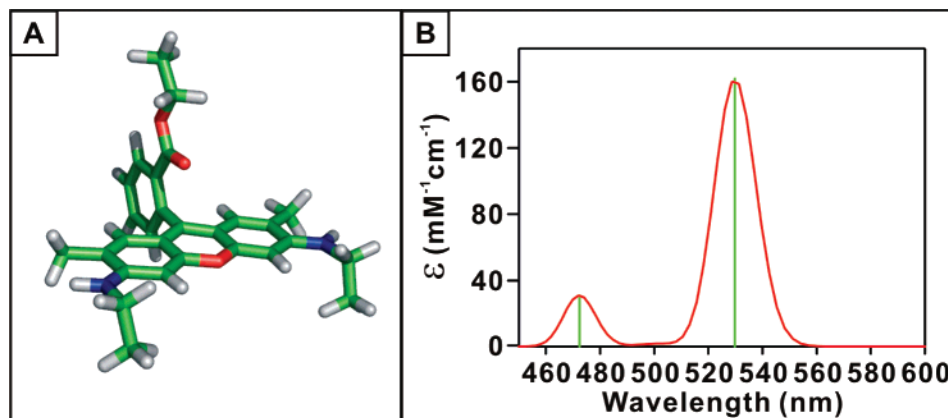(56) Jensen, L.; Schatz, G. C. *J. Phys. Chem. A* **2006**, *110*, 5973−5977.

Figure 10. Optimized structure and simulated absorption spectrum of R6G in solution. Solvent effects accounted for by a red-shift of 56 nm.
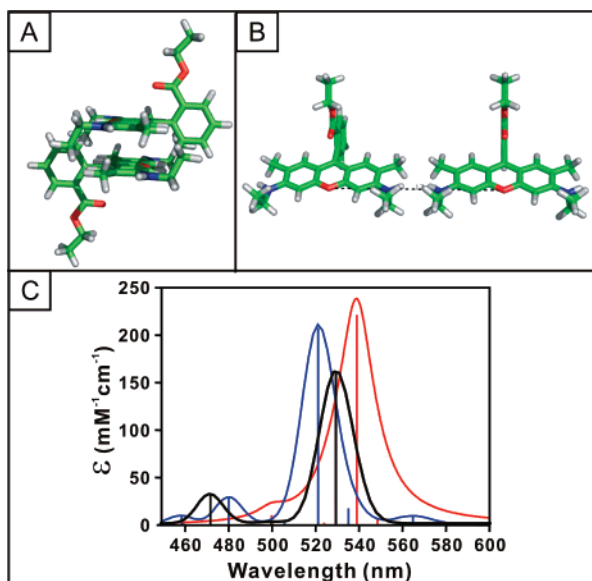

Figure 11. Simulated structure of R6G dimers and absorption spectra. (A) Structure of H-type dimer. (B) Structure of J-type dimer. (C) Calculated absorption spectra of R6G monomer (black line), H-type dimer (blue line), and J-type dimer (red line). Solution effects are accounted for by a red shift of 56 nm.

Figure 12. Simulated absorption spectra of R6G with a Ag$_2$ cluster and neutral R6G. (A) Calculated absorption of R6G with a Ag$_2$ cluster. (Inset) Optimized structure of R6G–Ag$_2$. The distance between the N atom of R6G and the Ag atom is 3.08 Å. (B) Calculated absorption of neutral R6G. Solution effects are accounted for by a red shift of 56 nm.

transfer transitions, arise when R6G adsorbs onto the metal surface. To examine this possibility we calculated the absorption spectrum of R6G interacting with an Ag$_2$ cluster (structure and spectrum shown in Figure 12A). The Ag$_2$ is used as a model for the adatom adsorption site. Because such a small cluster cannot represent the full effect of an Ag surface, we shifted the spectrum in Figure 12A by 56 nm. Therefore, the modeling should provide a reasonable description of the CT transitions. The interactions of R6G with the Ag$_2$ cluster cause a red-shift of the main transition to 544 nm, which is a 14-nm shift compared to that in solution. Two CT transitions to the red of the main peak are found at 1010 and 617 nm, corresponding to transitions from the HOMO of Ag$_2$ to the LUMO and LUMO+1 of R6G, respectively. Since both transitions have small oscillator strength and are more than 100 nm to the red of the main transition, it is not likely that they are responsible for the LSPR shift feature at ∼595 nm.

Another possibility is that the interaction between R6G and the surface may cause a complete charge transfer from the metal to R6G since it is a cationic dye. Therefore, we calculated the absorption spectrum of neutral R6G (see Figure 12B). The main
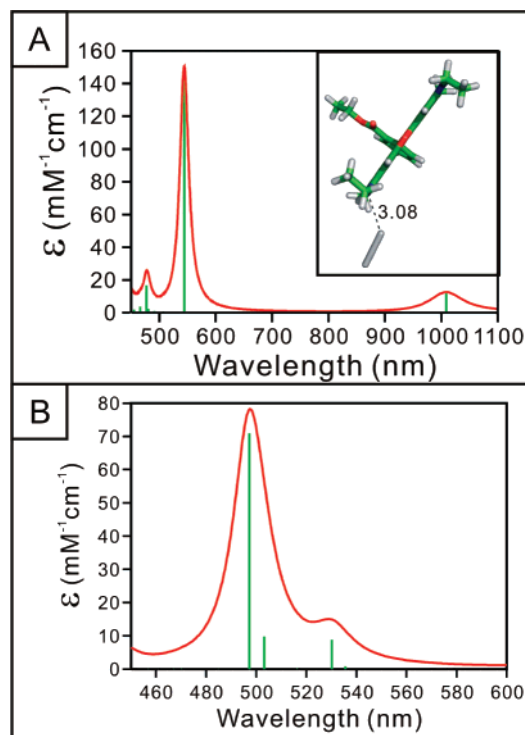
absorption peak is at 498 nm with a weaker band at around 530 nm. Both bands are blue-shifted relative to the cationic R6G absorption with smaller oscillator strength. This makes it unlikely that the formation of the neutral R6G is the cause for the LSPR shift feature at ∼595 nm.

The last explanation that we considered is that the adsorption of R6G onto the surface causes the angle, Ω, between the xanthene plane and the phenyl substituent to change (see Figure 13A for definition of Ω). Notice that the optimized structure of R6G (shown in Figure 10A) from the calculations has an angle of 88°, whereas in the experimental crystal structure R6G has an angle of 63°.[57] We calculated the absorption spectra of R6G as a function of Ω to show how the S$_0$–S$_1$ transition is sensitive

(57) Adhikesavalu, D. N.; Mastropaolo, D.; Camerman, A.; Camerman, N. *Acta Crystallogr., Sect. C* **2001**, *57*, 657–659.
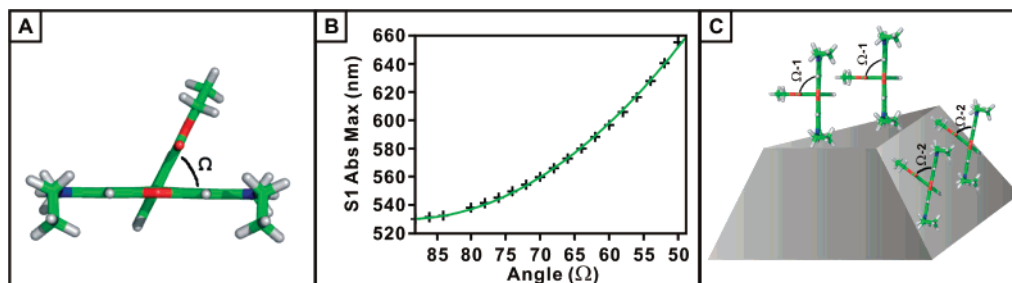
Figure 13. S_1 absorption maximum as a function of the angle (Ω) between the xanthene plane and the phenyl substituent. Solvent effects accounted for by a red shift of 56 nm. (A) Side view of the structure of R6G. (B) Plot of the S_1 absorption maximum as a function of the angle (Ω). (C) Schematic illustration of the two possible adsorption sites. $\Omega - 1 = 88°$, $\Omega - 2 = 66°$.

to the perturbation on the xanthene ring. The resulting absorption maximum of the S_0-S_1 transition is plotted (see Figure 13B) as a function of Ω. When Ω decreases, the excitation energy of the S_0-S_1 transition increases, leading to a red-shift of the main absorption peak. In order to explain the LSPR shift maximum at ~595 nm, an absorption feature around 570 nm is required. Figure 13B shows that such an absorption feature can be achieved when Ω is decreased by 20–25°. The corresponding Ω is then close to the value found for R6G in the crystal structure. The strain caused by decreasing Ω to this value amounts to ~15–17 kcal/mol. Furthermore, the strain reduces the oscillator strength of the S_0-S_1 transition. One could speculate that if two distinct absorption sites exist, for example, the top and sides of the NSL-nanoparticle (cartoon shown in Figure 13c), one of these sites could then cause Ω to twist, thereby red-shifting the S_0-S_1 transition. However, it requires a significant amount of energy to bend Ω by around 20–25°, making it a less likely explanation than the dimer formation.

Conclusions

The coupling between the R6G molecular resonances and the LSPR of Ag nanoparticles has been systematically probed. This is achieved by monitoring the shift in LSPR wavelength of Ag nanoparticles upon R6G binding. The LSPR shift depends on the relative spectral position between the LSPR of the Ag nanoparticles and the molecular resonances of R6G. The LSPR shifts show several complicated features—indeed three local maxima have been observed. In contrast, there are only two features in the R6G solution absorption spectrum. To understand the change in the R6G resonances when it adsorbs to metal surface, absorption spectra of R6G on an Ag surface have been measured at different R6G concentrations. Detailed deconvolution of the spectra indicates the formation of R6G dimers on the surface, even though the R6G concentration in solution is

low enough to avoid R6G aggregate formation in solution. To understand the unusual LSPR shifts, several different kinds of theoretical modeling were considered, including empirical modeling with dielectric constants from a Kramers–Kronig analysis, electrodynamics modeling using Gans theory, and electronic structure calculations using TDDFT. The combined experimental evidence and theoretical modeling show that dimer formation is responsible for the complex spectral coupling between R6G and the nanoparticles.

The extreme sensitivity of the localized surface plasmon resonance wavelength to small environmental changes has been clearly demonstrated in this work. For the first time, changes in the adsorbates' electronic structure due to aggregation have been detected using LSPR spectroscopy. These findings illustrate that the LSPR-sensing technique is particularly suitable for studying molecular level information, such as electronic and structural change of the adsorbates. This discovery has potential applications for chemical sensing, studying excited states at metal surfaces, understanding the mechanism of surface-enhanced Raman spectroscopy, and developing novel plasmonic devices.

Supporting Information Available: Refractive indices of R6G monomer, H-dimer, and J-dimer. This material is available free of charge via the Internet at http://pubs.acs.org.

JA0707106